

Endoplasmic reticulum: reduced and oxidized glutathione revisited

Julia Birk^{1,2}, Mariangela Meyer¹, Isabel Aller³, Henning G. Hansen⁴, Alex Odermatt^{1,2}, Tobias P. Dick⁵, Andreas J. Meyer³ and Christian Appenzeller-Herzog^{1,*}

¹Division of Molecular and Systems Toxicology, Department of Pharmaceutical Sciences, University of Basel, 4056 Basel, Switzerland

²Swiss Center for Applied Human Toxicology, University of Basel, 4056 Basel, Switzerland

³INRES – Chemical Signalling, University of Bonn, 53113 Bonn, Germany

⁴Department of Biology, University of Copenhagen, 2200 Copenhagen N, Denmark

⁵Division of Redox Regulation, DKFZ-ZMBH Alliance, German Cancer Research Center (DKFZ), 69120 Heidelberg, Germany

*Author for correspondence (Christian.Appenzeller@unibas.ch)

Accepted 28 January 2013

Journal of Cell Science 126, 1604–1617

© 2013. Published by The Company of Biologists Ltd

doi: 10.1242/jcs.117218

Summary

The reducing power of glutathione, expressed by its reduction potential E_{GSH} , is an accepted measure for redox conditions in a given cell compartment. In the endoplasmic reticulum (ER), E_{GSH} is less reducing than elsewhere in the cell. However, attempts to determine $E_{\text{GSH}}(\text{ER})$ have been inconsistent and based on ineligible assumptions. Using a codon-optimized and evidently glutathione-specific glutaredoxin-coupled redox-sensitive green fluorescent protein (roGFP) variant, we determined $E_{\text{GSH}}(\text{ER})$ in HeLa cells as -208 ± 4 mV (at pH 7.0). At variance with existing models, this is not oxidizing enough to maintain the known redox state of protein disulfide isomerase family enzymes. Live-cell microscopy confirmed ER hypo-oxidation upon inhibition of ER Ca^{2+} import. Conversely, stressing the ER with a glycosylation inhibitor did not lead to more reducing conditions, as reported for yeast. These results, which for the first time establish the oxidative capacity of glutathione in the ER, illustrate a context-dependent interplay between ER stress and $E_{\text{GSH}}(\text{ER})$. The reported development of ER-localized E_{GSH} sensors will enable more targeted *in vivo* redox analyses in ER-related disorders.

Key words: Endoplasmic reticulum, Glutathione, Green fluorescent protein, Reduction potential, Unfolded protein response

Introduction

The endoplasmic reticulum (ER) constitutes the starting point of the secretory pathway where secretory and membrane proteins are synthesized. Correct folding of these ER client proteins is required for their proper function, which critically depends on different ER-resident determinants such as chaperones, folding catalysts, ATP and Ca^{2+} levels (Braakman and Bulleid, 2011). Imbalances between the burden of protein synthesis in the ER and the capacity of its folding machinery activate an adaptive cellular program called the unfolded protein response (UPR), which is conserved from yeast to man (Hetz, 2012). The signaling pathways of the UPR, which include the phosphorylation of protein kinase RNA-like ER kinase (PERK) and eukaryotic initiation factor 2 α (eIF2 α) as well as the splicing of X-box binding protein 1 (XBP1) mRNA, mediate the transduction of information on the load of unfolded proteins (so-called ‘ER stress’) from the ER lumen to cytosol and nucleus.

Protein homeostasis in the ER is strongly connected to the formation of native disulfide bonds during client protein folding, which also requires reduction of non-native bonds (Braakman and Bulleid, 2011). Important catalysts of these thiol–disulfide exchange reactions are the members of the protein disulfide isomerase (PDI) family. Upstream of PDIs, endoplasmic oxidoreductin 1 (Ero1) enzymes, among other pathways (Ruddock, 2012), generate disulfide bonds by reducing molecular oxygen (Ramming and Appenzeller-Herzog, 2012).

This oxidative mechanism is antagonized by the low molecular weight thiol compound glutathione (GSH), which maintains a reduced fraction of PDIs (Chakravarthi et al., 2006). GSH-mediated reduction results in the formation of its dimeric oxidized form glutathione disulfide (GSSG). The presence of oxidizing and reducing components in the ER allows a dynamic control of the redox state (Appenzeller-Herzog, 2011).

The status of the glutathione redox couple (GSH–GSSG) is an accepted indicator of intracellular redox conditions (Schafer and Buettner, 2001). For instance, compared to the cytosol, the GSH:GSSG ratio in the ER is significantly lower (Hwang et al., 1992; Appenzeller-Herzog, 2011). In keeping with this, glutathione is mainly transported through the ER membrane in its reduced form, whereas GSSG is retained and accumulated in the ER lumen (Bánhegyi et al., 1999). Unfortunately, there is wide disagreement in the literature as to the actual oxidative capacity, i.e. the electrochemical reduction potential of GSH–GSSG (E_{GSH}) in the ER (Hwang et al., 1992; Dixon et al., 2008; van Lith et al., 2011; Delic et al., 2012; Kolossov et al., 2012), which is given by the Nernst equation (see below). One reason for this is that it is not possible to deduce E_{GSH} from the GSH:GSSG ratio alone without knowledge of the absolute glutathione concentration (Appenzeller-Herzog, 2011).

Green fluorescent protein (GFP) is a jellyfish protein of 26.9 kDa emitting bright green light when excited with light around 480 nm (Shimomura et al., 1962). The chromophore of

wild type GFP (wtGFP) is formed by the three amino acids Ser⁶⁵, Tyr⁶⁶ and Gly⁶⁷. It exhibits two excitation peaks at 395 nm and 475 nm, the molecular reason of which is the reversible protonation of Tyr⁶⁶ (Brejč et al., 1997). Critical improvements in expression and brightness of GFP in mammalian cells were achieved by substitution of Ser⁶⁵ with threonine and by systematic codon optimization (Yang et al., 1996). These alterations led to a new GFP variant called enhanced GFP (EGFP).

In order to obtain two variants of redox-sensitive GFP (designated roGFP1 and 2), Ser¹⁴⁷ and Gln²⁰⁴ were replaced by cysteines, which allowed formation of a disulfide bond under oxidizing conditions (Dooley et al., 2004; Hanson et al., 2004). Formation and dissolution of this disulfide influences the protonation of Tyr⁶⁶, thus rendering roGFP a ratiometric sensor, which exhibits redox-dependent changes in emission intensity following excitation at two different wavelengths (Meyer and Dick, 2010). RoGFP-based probes have extensively been used in mitochondria and cytosol (Meyer and Dick, 2010) where they specifically sense E_{GSH}. This specificity, which has first been described for the related rxYFP sensor (Østergaard et al., 2004), depends on the expression of endogenous glutaredoxins, which catalyze thiol–disulfide exchange between the GSH–GSSG and roGFP redox pairs (Meyer et al., 2007). Based on this principle, cytosolic and mitochondrial E_{GSH} sensors of high responsiveness and specificity have been created by intramolecular fusion of human glutaredoxin-1 (Grx1) to roGFP2 (Gutscher et al., 2008). Redox measurements using roGFPs targeted to the ER have also been reported. In contrast to roGFP2 (Merksamer et al., 2008), modified, more oxidizing variants based on roGFP1 (Lohman and Remington, 2008) were found not to be quantitatively oxidized at steady state in the ER (Zito et al., 2010; van Lith et al., 2011; Delic et al., 2012). However, since no endogenous glutaredoxins are expressed in the ER of human cells (Izquierdo et al., 2008), the specificity of any roGFP variant in this compartment is unclear.

On these grounds, we expressed ER-targeted and codon-optimized fusion proteins of Grx1 and different roGFP variants with the aim to determine E_{GSH} in the ER [E_{GSH}(ER)]. Indeed, the steady-state redox distribution of Grx1-coupled roGFP was significantly more oxidized than that of their uncoupled

counterparts, indicating that the latter were not in equilibrium with GSH–GSSG. Deduced values for E_{GSH}(ER) prompt the reassessment of existing models.

Results

Constructing improved ER-targeted roGFP variants

RoGFP sensors have been found to monitor E_{GSH} in the cytosol, and their specific response depends on catalysis of their reaction with GSH–GSSG by endogenous glutaredoxins (Meyer et al., 2007). However, there is no evidence for expression of any glutaredoxins in the non-fungal ER (Izquierdo et al., 2008), and the switch disulfide in conventional roGFPs is so stable [E_{1/2} < –270 mV (Meyer and Dick, 2010)] that the reduced dithiol form is virtually absent under steady-state conditions in the oxidizing environment of the ER (Merksamer et al., 2008) (and see below). We therefore used roGFP variants carrying amino acid insertions adjacent to Cys¹⁴⁷ (termed roGFP-iX where X denotes the inserted amino acid in single letter code), which display a substantially lowered thermodynamic stability of the switch disulfide, resulting in midpoint potentials that range between –229 and –246 mV (Lohman and Remington, 2008). Furthermore, to enable equilibration of the probes with GSH–GSSG specifically we also expressed roGFP-iX probes as Grx1 fusion proteins in the ER (Fig. 1A). Expression of Grx1 in the ER led to artifactual N-glycosylation of a consensus site at position 52 (supplementary material Fig. S1), which is located in a solvent exposed loop ~16 Å away from the active site (Sun et al., 1998). However, since comparison with a glycosylation-site mutant revealed that neither the folding of the sensor nor the catalysis of thiol–disulfide exchange between roGFP and GSH–GSSG was inhibited by glycosylation (see below, supplementary material Fig. S4B; Fig. S7A), we proceeded with the glycosylated variants.

Initially, we fused HA-tagged roGFP1-iE, derived from the original jellyfish wtGFP cDNA (Lohman and Remington, 2008), to an N-terminal signal peptide and a C-terminal ER retrieval motif (roGFP1-iE_{ER}) (Fig. 1A). Although similar constructs have previously been published (Zito et al., 2010; van Lith et al., 2011), this probe was found to be poorly expressed (Fig. 1B) and difficult to detect by fluorescence readouts (supplementary material Fig. S2). Comparable results were obtained with

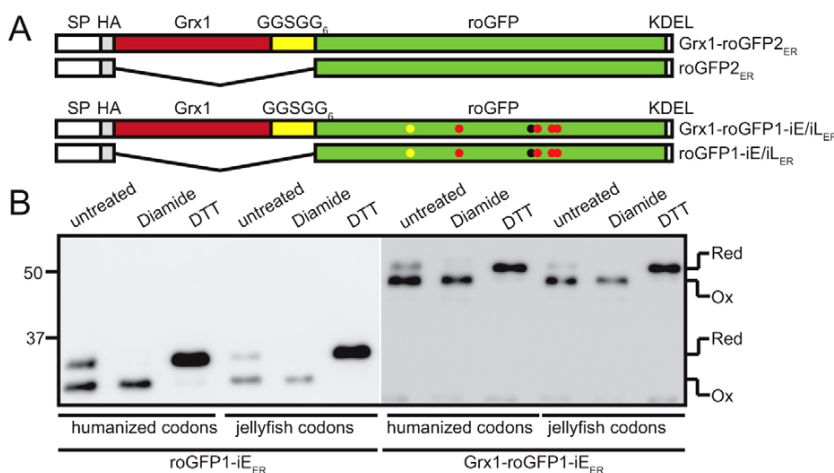


Fig. 1. Improved roGFP sensors targeted to the ER.

(A) Schematic representation of the roGFP_{ER} sensors Grx1-roGFP2_{ER}/roGFP2_{ER} (top), and Grx1-roGFP1-iE_{ER}/roGFP1-iE_{ER} (bottom) used in the present study. SP, ER signal peptide; HA, hemagglutinin epitope; GGSGG₆, glycine–serine linker. The roGFP1-iX probes were generated from the roGFP2 probes by introducing the indicated mutations: yellow dot, T65S mutation; red dots, folding mutations F99S, M153T, V163A and I167T; black dot, E or L insertion at position 147a and H148S. (B) HeLa cells expressing roGFP1-iE_{ER} or Grx1-roGFP1-iE_{ER} with either humanized or jellyfish codons were subjected to anti-GFP IP followed by non-reducing SDS-PAGE and anti-HA WB. Where indicated, cells were oxidized with diamide or reduced with DTT prior to treatment with NEM and cell lysis. The positions of marker proteins are indicated in kDa, and the mobilities of oxidized (Ox) and reduced (Red) roGFPs are labeled.

wtGFP-derived Grx1-roGFP-iE_{ER} (Fig. 1B; supplementary material Fig. S2).

We therefore equipped EGFP-based roGFP2 and Grx1-roGFP2 constructs (Gutscher et al., 2008) with ER-targeting sequences and HA-epitope and subsequently introduced the iE or iL insertion. In addition, to precisely match the roGFP1-iX amino acid sequence (Lohman and Remington, 2008), we replaced Thr⁶⁵ with serine and introduced the 'folding mutations' F99S, M153T, V163A and I167T (Fig. 1A). Of note, Ser versus Thr in position 65 defines the principal difference between wtGFP/roGFP1 and EGFP/roGFP2. The roGFP2 constructs, which are composed of high-usage ('humanized') codons for expression in mammalian cells, were thus converted into roGFP1-iX and Grx1-roGFP1-iX constructs with proper codon composition. These readily showed a reticular fluorescence pattern that colocalized with PDI, a bona fide ER marker (supplementary material Fig. S3). Consistent with the literature (Haas et al., 1996; Yang et al., 1996), comparison of the humanized roGFP1-iE_{ER} constructs with the wtGFP-based constructs by western blot (WB) documented enhanced expression of the former (Fig. 1B). As expected for two sensors with the same amino acid sequence, the steady-state degree of probe oxidation in the ER was not influenced by the codon composition of the construct (Fig. 1B).

Folding of roGFP-iX sensors in the ER is hampered

Formation of the switch disulfide in roGFP, which bridges two neighboring strands in the native GFP β -barrel (Meyer and Dick, 2010), likely reflects the correct conformation of the protein and can be easily monitored by non-reducing SDS-PAGE (Fig. 1B). Hence, we monitored the folding rate of different roGFP_{ER} variants by pulse-chase analysis. While roGFP2_{ER} and Grx1-roGFP2_{ER} (Fig. 1A) were readily folded, acquisition of the correct conformation was delayed for all roGFP1-iX_{ER} constructs (supplementary material Fig. S4A). This delay was most prominent for roGFP1-iL_{ER}.

Evidence for hampered folding of iX variants in the ER was also obtained, when analyzing the sensors by WB. Here, the proportion of reduced sensor was significantly higher in cell lysates than in corresponding immunoprecipitates (supplementary material Fig. S4C). This higher proportion of the oxidized form corresponded better to the results obtained by fluorescence measurements (see below). This suggested that the reduced fraction in cell lysates contained misfolded (i.e. non-oxidizable) roGFP-iX, which was removed by the centrifugation step of the immunoprecipitation (IP) procedure. Also for roGFP2_{ER} and Grx1-roGFP2_{ER}, a minor reduced fraction was visible in whole-cell lysates (supplementary material Fig. S4D).

Does the low folding efficiency of roGFP1-iX_{ER} variants affect their performance as real-time redox sensors, i.e. their responsiveness to changes in redox? In a previous study (van Lith et al., 2011) on cells expressing roGFP1-iL in the ER, recovery of the reduced fraction of the sensor occurred only very slowly upon washout of the oxidant 2,2'-dithiodipyridine (DPS). To recapitulate this, we subjected cells transfected with roGFP1-iX_{ER} sensors to a similar washout procedure using either diamide or DPS as the oxidant and analyzed the redox state of the sensors at different time points after washout by IP and WB. As shown in Fig. 2A and supplementary material Fig. S5, both Grx1-fused and unfused roGFP1-iX_{ER} readily recovered from diamide/DPS-induced hyperoxidation at a rate comparable to the recovery rates of endogenous PDIs (Appenzeller-Herzog et al., 2010).

Likewise, oxidative recovery of roGFP1-iX_{ER} sensors following washout of the reductant dithiothreitol (DTT) occurred promptly (van Lith et al., 2011) (see below). To probe for their ability to report modest redox changes, we also incubated (Grx1-)roGFP1-iE_{ER}-expressing cells in a range of concentrations of DTT or diamide and determined their redox state by IP and WB. Consistent with what has been observed with roGFP-iL (van Lith et al., 2011), the sensors readily responded to submillimolar concentrations of reductant/oxidant (Fig. 2B). Taken together, although initial folding of roGFP1-iX_{ER} variants appears to be relatively inefficient, they are, once properly folded, capable of reporting redox changes in the ER.

Different roGFP_{ER} variants show distinct behaviors

We next quantified the steady-state redox state of the four ER-targeted roGFP1-iX sensors as well as of Grx1-roGFP2_{ER} in transiently transfected HeLa cells using three independent techniques: *in situ* fluorescence spectrum analysis, IP/WB, and ratiometric live-cell fluorescence microscopy. For fluorescence spectrum analysis in a plate reader, transfected cells were trypsinized and seeded into 96 well plates. To obtain oxidized or reduced control spectra, cells in some wells were treated with DPS or DTT. As expected, Grx1-roGFP2_{ER} was fully oxidized in the ER ($99 \pm 0.5\%$) (Fig. 3A,B). Conversely, roGFP1-iX_{ER} sensors produced excitation spectra, in which the curve recorded from untreated cells clearly ran intermediate to the curves recorded from oxidized and reduced cells (Fig. 3A). In general, the fluorescence signals from iL sensors were weaker compared to the ones from iE sensors. This was particularly evident for roGFP1-iL_{ER}, which yielded a low-quality spectrum (Fig. 3A) with limited reproducibility (Fig. 3B). Interestingly, at steady-state Grx1-roGFP1-iE_{ER} was more oxidized ($91 \pm 3\%$) than roGFP1-iE_{ER} ($82 \pm 7\%$).

The redox states of all sensors were also examined by IP and WB. Again, all roGFP1-iX_{ER} sensors displayed a characteristic distribution of reduced and oxidized species, whereas Grx1-roGFP2_{ER} was fully oxidized (Fig. 4A). As in the excitation spectrum analyses (Fig. 3), roGFP1-iE_{ER} was less oxidized ($54 \pm 1\%$) than Grx1-roGFP1-iE_{ER} ($70 \pm 5\%$) (Fig. 4B). Probably owing to incomplete removal of the misfolded subfraction (see supplementary material Fig. S4), the WB readout yielded slightly more reduced redox distributions than fluorescence scanning. Compared to iE variants, iL variants consistently formed more high-molecular weight complexes of unknown identity. Accordingly, the reduced and oxidized monomeric forms of iL variants were less prominently detected compared to iE (Fig. 4A), which correlated with their weaker fluorescence (Fig. 3). Altogether, the data so far indicated roGFP1-iE_{ER} and Grx1-roGFP1-iE_{ER} to be the most reliable ER redox sensors.

To complement the above results with a data set, which also reports cell-to-cell differences, we next turned to live imaging of single cells. Due to poor fluorescence of roGFP1-iL_{ER} variants, these analyses were focused on the variants carrying the iE insertion. Transfected cells were subjected to laser scanning microscopy using two different laser lines for excitation. To obtain the excitation ratio corresponding to unperturbed, fully oxidized, and fully reduced sensor, the cells were first imaged at steady state and then treated with 0.5 mM diamide followed by addition of 20 mM DTT. Calculation of the steady-state redox distributions yielded numbers that were comparable to the results

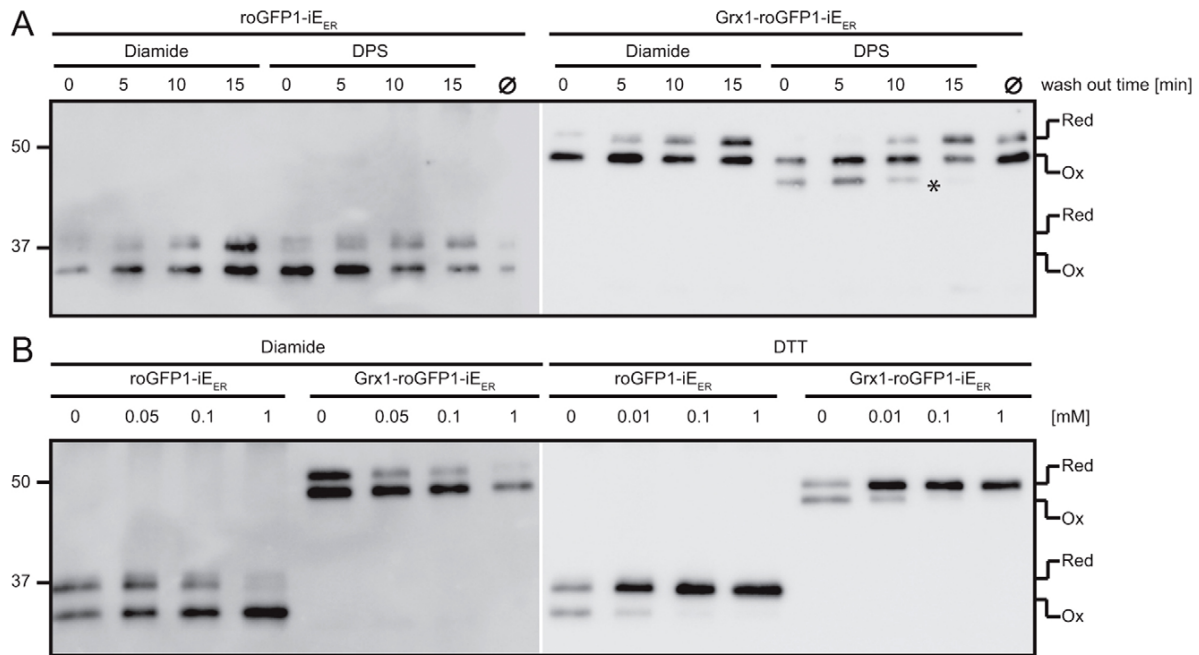


Fig. 2. Folded roGFP_{ER} variants are responsive to redox changes in the ER. (A) Transiently transfected HeLa cells were incubated with diamide or DPS, and the oxidants were washed out for 0, 5, 10 or 15 min. The oxidation state of cysteines was blocked with NEM and the samples processed as in Fig. 1B. (B) Indicated concentrations of DTT or diamide in HEPES buffer were applied to HeLa cells expressing roGFP1-iE_{ER} or Grx1-roGFP1-iE_{ER}. A fresh DTT stock solution was calibrated as described previously (Appenzeller-Herzog et al., 2010). One of two independent experiments is shown. Mobilities of oxidized and reduced sensors are indicated. Asterisk, unidentified, DPS-dependent redox form of Grx1-roGFP_{ER}-iE.

obtained by fluorescence spectrum analysis. As shown in Fig. 5, Grx1-roGFP_{2ER} was completely oxidized. By contrast, the oxidized fractions of roGFP1-iE_{ER} and Grx1-roGFP1-iE_{ER} were $82 \pm 13\%$ and $93 \pm 2\%$, respectively (Fig. 5B). For unknown reasons, variations in the excitation ratio between individual cells were only evident at steady state and under oxidizing conditions, but disappeared upon reduction of the sample (Fig. 5A).

Taken together, the results in Figs 3–5 confirmed the previously described effects caused by amino acid insertions on the stability of the disulfide bridge in roGFP1 (Lohman and Remington, 2008). Moreover, N-terminal fusion of Grx1 led to increased oxidation of roGFP1-iE in the ER at steady state.

Grx1 does not hyperoxidize the ER but modulates the redox characteristics of roGFP1-iE

Since Grx is normally absent from the ER, the finding that fusion of Grx1 to roGFP1-iE_{ER} increases its steady-state oxidation could potentially be explained by Grx1-mediated changes in overall ER redox conditions, which would be expected to elicit the UPR (Hansen et al., 2012). We therefore set out to test these possibilities.

First, the ability of the newly developed sensors to report oxidative changes in the ER was examined. For this purpose, we generated a cell line overexpressing a hyperactive form of Ero1 β (Ero1 β -C100/130A) (Wang et al., 2011) under a doxycycline-inducible promoter. Compared to wild-type Ero1 β , induction of hyperactive Ero1 β for 24 h caused increased oxidation of the ER-resident protein ERp57 (Fig. 6A). ER hyperoxidation by Ero1 β -C100/130A was also evident when analyzing the redox states of

roGFP1-iE_{ER} or Grx1-roGFP1-iE_{ER}, the sensors with the least oxidized steady-state distribution in the ER (Fig. 2), by IP/WB (Fig. 6B) (Grx1-roGFP1-iE_{ER} was omitted because of its already high steady-state oxidation and roGFP1-iE_{ER} because of its poor folding; see above). Unfortunately, fluorescent readouts in this setup were not possible owing to the fluorescence of doxycycline.

We next checked whether expression of Grx1 in the ER showed effects comparable to those of Ero1 β -C100/130A, which could explain the observed differences between roGFP1-iE_{ER} and Grx1-roGFP1-iE_{ER}. For this purpose, we transfected cells with the different roGFP_{ER} sensors, with ER-localized Grx1 (Grx1_{ER}; supplementary material Fig. S6), or with Ero1 β -C100/130A and determined the redox state of endogenous ERp57. In contrast to Ero1 β -C100/130A, neither roGFPs nor Grx1_{ER} affected the redox state of ERp57 (Fig. 6C). Likewise, Grx1_{ER} did not influence the redox state of HyPer_{ER} (Fig. 6D), a ratiometric probe, which reacts with H₂O₂ (Belousov et al., 2006; Enyedi et al., 2010) and, probably, with PDIs (Ruddock, 2012). To monitor possible signs of Grx1-dependent ER stress, we analyzed markers of the UPR and found that neither Grx1-fused roGFP_{ER} sensors nor Grx1_{ER} by itself elicited UPR signaling (Fig. 6E). We concluded that expression of Grx1 in the ER does not broadly affect ER redox homeostasis. The formal possibility that Grx1 catalyzes deglutathionylation of ER proteins, which would increase GSSG levels in the ER, can at present not be excluded. However, we consider this possibility unlikely, because (i) the abundance of glutathionylated ER proteins is low (Hansen et al., 2009) and (ii) unnaturally increased GSSG levels would elicit the UPR (Hansen et al., 2012).

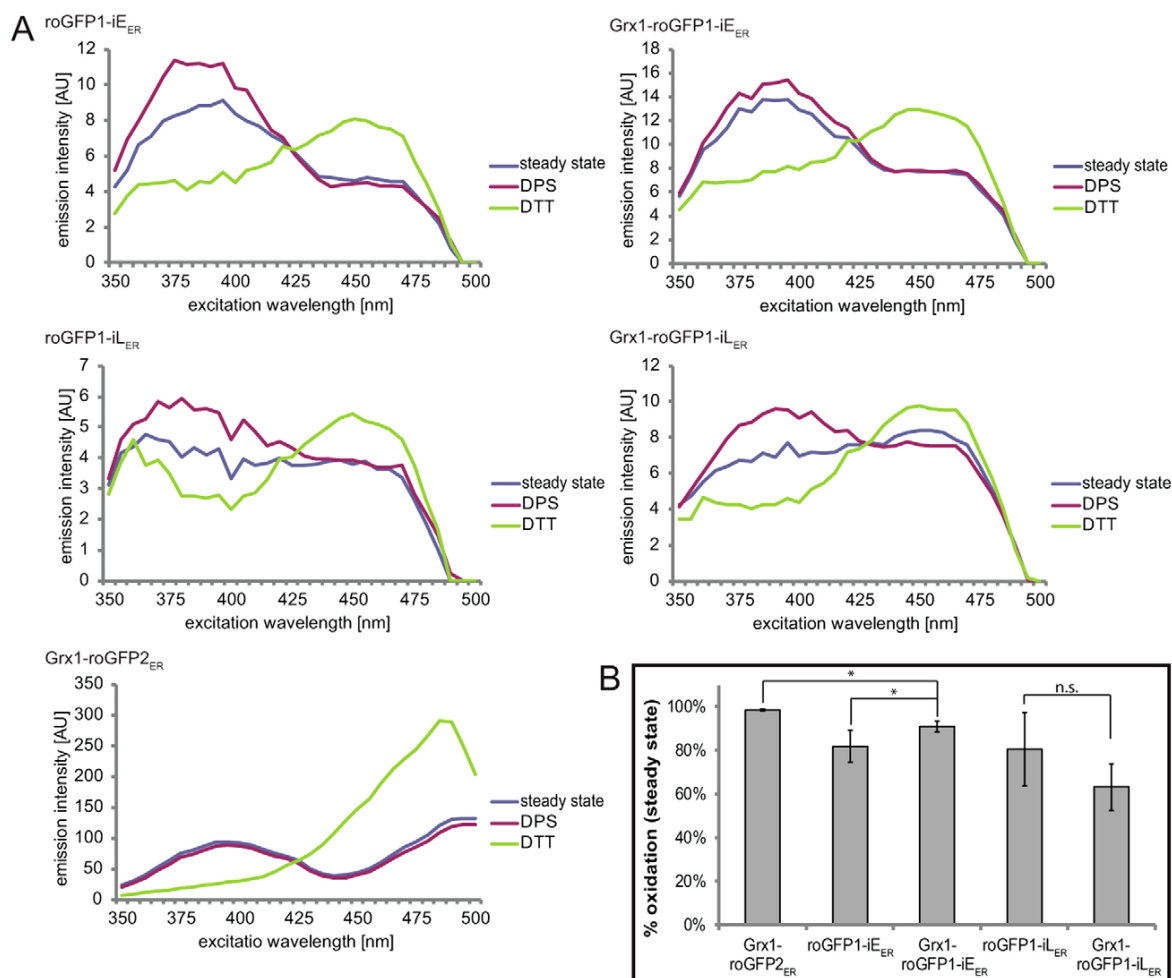


Fig. 3. Excitation spectrum analysis of roGFP_{ER} sensors. Transiently transfected HeLa cells were trypsinized, resuspended in HEPES buffer, mock-, DPS- or DTT-treated, and subjected to fluorescence spectrum analysis. (A) Representative *in situ* spectra of each sensor at steady state (blue), full oxidation (red) or reduction (green). AU, arbitrary units. (B) The degree of oxidation of the sensors as a percentage was calculated from emission intensities at 400 and 490 nm (roGFP_{ER}) and at 390 and 465 nm (roGFP1-iX_{ER}) excitation, respectively (average \pm s.d.; $n \geq 3$). Asterisks indicate statistical significance ($P < 0.03$). n.s., not significant.

We next examined whether the increased oxidation of Grx1-roGFP1-iE in the ER could be the result of altered redox properties of this sensor compared to roGFP1-iE. Thus, the midpoint reduction potentials E° of Grx1-fused and unfused sensors were determined using purified proteins. Consistent with published data (Lohman and Remington, 2008), $E^{\circ}_{\text{roGFP1-iE}}$ was -233 ± 5 mV (Fig. 6F). However, N-terminal fusion of Grx1 resulted in a slightly more reducing E° of -239 ± 3 mV (Fig. 6G), which may partially explain the observed differences in ER sensor oxidation.

Grx1 catalyzes thiol-disulfide exchange between roGFP and GSH-GSSG in the ER

Reaction of Grx1-roGFP1-iE with glutathione *in vitro* was markedly accelerated compared to roGFP1-iE (Fig. 7A), thus confirming previous findings with the N-terminal fusion of Grx1 to roGFP2 (Gutscher et al., 2008). To examine whether such catalysis also occurs in the ER, we exploited the fact that ER

GSSG levels readily rise after DTT treatment and rapid washout (Appenzeller-Herzog et al., 2010). Thus, DTT recovery assays using cells transfected with roGFP_{ER} variants with or without fused Grx1 were performed and analyzed by IP/WB. Indeed, recovery of roGFP2_{ER} was accelerated by the addition of Grx1 (Fig. 7B). The overall rapidity of roGFP2_{ER} re-oxidation is presumably determined by the strong sensitivity of this sensor to trace amounts of GSSG (Gutscher et al., 2008). Likewise, the re-oxidation of Grx1-roGFP1-iE_{ER}, which occurred in the time scale of minutes, was faster than that of roGFP1-iE_{ER} (Fig. 7C). Grx1-mediated acceleration was not influenced by mutation of its glycosylation site, but depended on active-site cysteines (supplementary material Fig. S7). Mutation of the active site in Grx1 also significantly lowered the steady-state oxidation of Grx1-roGFP1-iE_{ER} (Fig. 7D,E). These results demonstrated that the catalytic activity of Grx1 specifically enhanced the equilibration of Grx1-roGFP1-iE_{ER} with GSH-GSSG.

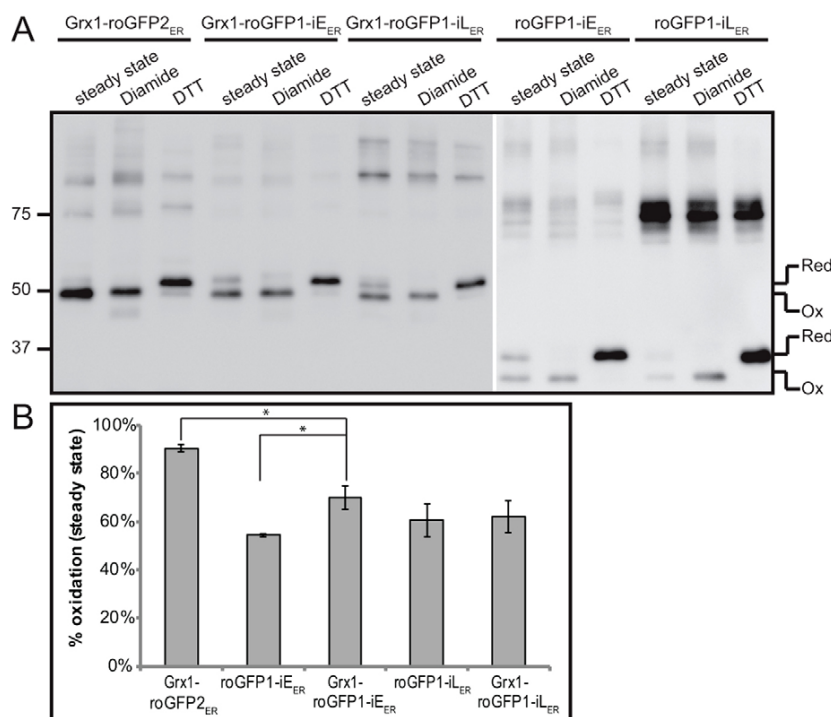


Fig. 4. RoGFP1-iE_{ER} and Grx1-roGFP1-iE_{ER} are best suited as ER redox sensors. (A) Transiently transfected HeLa cells were processed as in Fig. 1B. (B) Densitometric quantification of the degree of (monomeric) sensor oxidation as a percentage (average \pm s.d.; $n=3$). Asterisks indicate statistical significance ($P<0.02$).

Based on these findings and assuming that Grx1-roGFP1-iE_{ER} is in (quasi-)redox equilibrium with GSH–GSSG, we then calculated $E_{\text{GSH}}(\text{ER})$ from $E^{\circ}_{\text{Grx1-roGFP1-iE}} = -239$ mV and the steady-state redox state of Grx1-roGFP1-iE_{ER} by using the Nernst equation. As we figured the fluorescent fraction of the sensor to be correctly folded, we considered the numbers obtained by fluorescence spectrum analysis (Fig. 3) and laser scanning microscopy (Fig. 5) the most reliable, which yielded values for $E_{\text{GSH}}(\text{ER})$ at pH 7.0 of -209 ± 4 mV and -205 ± 3 mV, respectively.

The relationship between ER stress and ER redox is non-linear

Having established two *in situ* sensor molecules, one of which specifically reports $E_{\text{GSH}}(\text{ER})$ (Grx1-roGFP1-iE_{ER}) and the other the redox state of (an) as yet ill-defined ER redox pair(s) (roGFP1-iE_{ER}; see Discussion), we set out to examine the relationship between induction of ER stress and redox state in real-time experiments. Since DTT elicits ER stress via manipulation of ER redox and the membrane trafficking inhibitor brefeldin A was found to impede accurate time-lapse analyses, we concentrated our investigations on the well-established ER stress inducers thapsigargin (TG, an ER Ca^{2+} pump inhibitor) and tunicamycin (TM, an inhibitor of glycosylation).

Recent data by Enyedi et al. (Enyedi et al., 2010) using TG and the HyPer_{ER} probe demonstrated that lowered ER Ca^{2+} content promptly diminishes oxidation of the HyPer probe in the ER. Since the underlying mechanism is obscure and TG-mediated hypo-oxidation may be restricted to the $\text{H}_2\text{O}-\text{H}_2\text{O}_2$ redox couple (as potentially measured by HyPer_{ER}), we were interested whether inhibition of the Ca^{2+} pump would also have an influence on GSH–GSSG. As published (Enyedi et al., 2010),

real-time monitoring indicated a prominent reduction of the HyPer_{ER} redox state upon addition of TG, which occurred within 5 minutes (Fig. 8A). RoGFP1-iE_{ER} as well as Grx1-roGFP1-iE_{ER} showed a very similar behavior, suggesting that TG-induced Ca^{2+} depletion from the ER broadly influences thiol–disulfide equilibria in the ER. As expected for the highly reducing roGFP2 sensor (Meyer and Dick, 2010), addition of TG to cells expressing Grx1-roGFP2_{ER} did not elicit any change in fluorescence.

Since treatment of yeast cells with TM causes pronounced under-oxidation of ER-targeted roGFP2 after a lag time of 1 h (Merksamer et al., 2008), we tested whether this was also the case in mammalian cells using roGFP1-iE_{ER}. However, no reduction of the sensor was observed in HeLa cells even 6 h after the application of TM (Fig. 8B). Conversely, a subset of cells manifested a slight hyperoxidation of roGFP1-iE_{ER}, which started roughly 100 min after TM addition. We concluded that the relationship between ER stress and ER redox is likely indirect and depends on the context.

Discussion

Using a glutathione-specific ER-targeted redox sensor, our work provides quantitative data to resolve the long-standing question of how oxidizing the ER is. Based on data from two independent fluorescence readouts, we determined $E_{\text{GSH}}(\text{ER})$ in HeLa cells to be -208 ± 4 mV (at pH 7.0), which, as expected, is more oxidizing than $E_{\text{GSH}}(\text{cytosol})$ of ~ -300 mV (Gutscher et al., 2008). Given the necessity for both oxidative and reductive processes in the ER (Braakman and Bulleid, 2011) and the central position of this organelle in many physiological and pathological processes (Rutkowski and Hegde, 2010; Hetz, 2012), this knowledge is of broad relevance.

Initial evidence for a relatively oxidizing E_{GSH} in the ER/secretory pathway was obtained twenty years ago in hybridoma cells (Hwang et al., 1992). Using a membrane-permeable tetrapeptide, which was glycosylated and trapped in the secretory pathway and which reacted *in situ* with GSH–GSSG,

the authors elegantly demonstrated a more oxidized GSH:GSSG ratio in secretory compartments compared to the overall ratio in the whole cell. By estimating cell volume and glutathione concentration, the deduced GSH:GSSG ratios between 1:1 and 3:1 led to an estimate of E_{GSH} between -172 and -188 mV (Hwang et al., 1992). The accuracy of these numbers, however, depends on the validity of several bold assumptions, in particular (i) that the tetrapeptide probe specifically and fully equilibrated with GSH–GSSG and (ii) that the glutathione concentration in the secretory pathway equaled the overall cellular concentration. Many years later, GSH was derivatized in rat liver microsomes, and the GSH:GSSG ratio determined with comparable results to the Hwang study (Bass et al., 2004). However, as microsomes are permeable to GSH (Bánhegyi et al., 1999), the significance of these results is unclear. Indeed, it was later shown that perfusion of livers with the sulfhydryl-modifying agent iodoacetic acid (IAA) prior to preparation of microsomes resulted in intramicrosomal GSH:GSSG ratios of up to 6:1 (Dixon et al., 2008). Still, whether in this setup, leakage of GSH was fully prevented by IAA was not shown, and a further confounding factor is the poor membrane permeability of IAA (Hansen and Winther, 2009).

More recent estimates of $E_{\text{GSH}}(\text{ER})$ were obtained using GFP-based sensors in the ER. By monitoring roGFP1-iE in the ER of the yeast *Pichia pastoris*, $E_{\text{GSH}}(\text{ER})$ was suggested to be -242 mV (Delic et al., 2012). A similar value (-231 mV) was obtained in human HT1080 cells stably transfected with ER-targeted roGFP1-iL (van Lith et al., 2011). Conversely, the most oxidizing value in the spectrum of suggested reduction potentials of the ER (-118 mV) was obtained using an engineered, redox-sensitive Förster resonance energy transfer sensor protein (Kolossova et al., 2012). These inconsistent outcomes apparently reinforce the concept that multiple ER redox couples, which are kinetically separated from each other, exist in parallel (Appenzeller-Herzog, 2012). Considering the high concentration of glutathione ($[\text{GSx}]_{\text{ER}}$, see below) though, E_{GSH} is probably the most accurate measure for the degree of ER oxidation, as has also been suggested by others (Schafer and Buettner, 2001).

In this study, we report that appending Grx1 to roGFP1-iE_{ER} conferred specificity towards GSH–GSSG (Fig. 7), which was exploited to measure E_{GSH} as -208 mV. {In terms of absolute reduction potential, it is important to consider that pH(ER) is probably slightly above 7.0. Thus, since $\text{pK}_{\text{aGrx1-roGFP1-iE}} > 8$ (our unpublished data), $E^{\circ}_{\text{Grx1-roGFP1-iE}}$ (and therefore also E_{GSH}) decreases by 6 mV/0.1 pH unit (Schafer and Buettner, 2001).} Although roGFP1-iE_{ER} by itself may also to some extent interact with GSH–GSSG, its redox state was highly variable in our hands, as indicated by large standard deviations (Figs 3, 5). Moreover, its theoretical redox state assuming quasi-equilibration with GSH–GSSG (as calculated with E_{GSH} and $E^{\circ}_{\text{roGFP1-iE}}$) is

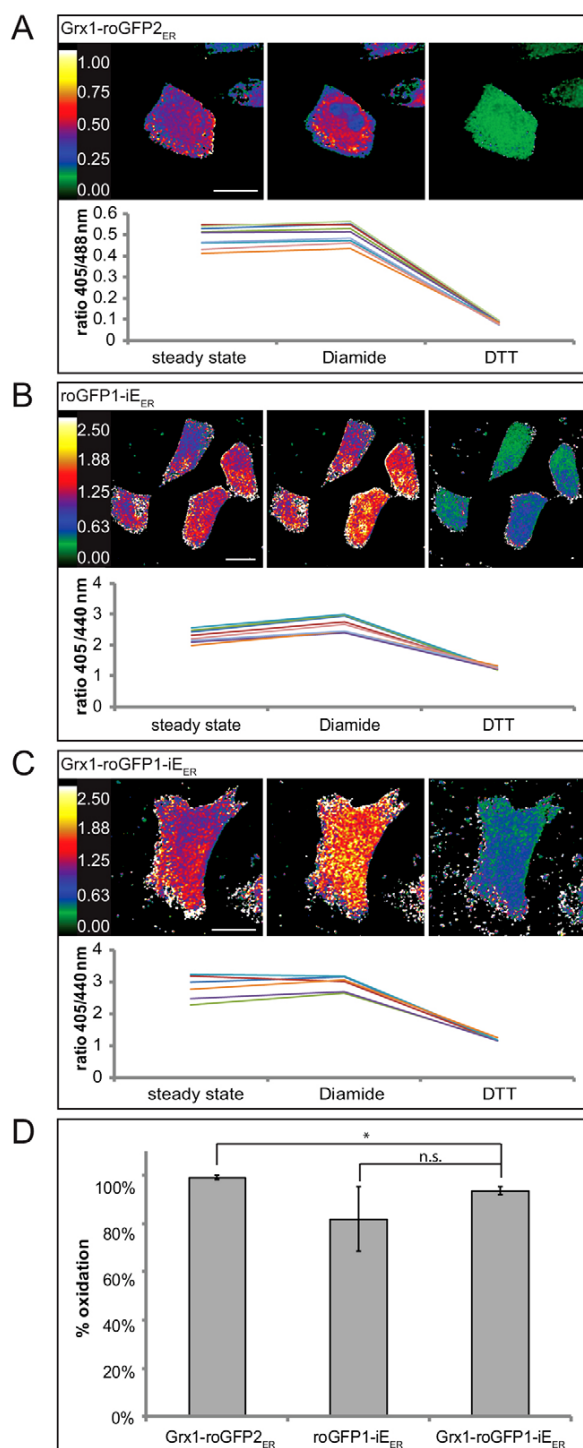


Fig. 5. Confocal live-cell imaging of roGFP_{ER} sensors. HeLa cells expressing Grx1-roGFP2_{ER} (A), roGFP1-iE_{ER} (B) or Grx1-roGFP1-iE_{ER} (C) were imaged by ratiometric laser scanning microscopy at steady state and upon sequential addition of diamide and DTT. The ratios of emission intensities (405 nm excitation:488 or 440 nm excitation) obtained from individual cells are plotted along with a representative false colour image. Scale bar: 20 μm . (D) Quantification of the degree of oxidation of the sensor at steady state as a percentage (average \pm s.d.; three independent experiments/micrographs with several cells analyzed in each). The asterisk indicates statistical significance ($P < 0.02$). n.s., not significant.

87% oxidized, which clearly diverges from the measured average value of 82% (Figs 3, 5). We therefore believe that roGFP1-iE_{ER} does not preferentially react with the glutathione redox couple

but also with other redox partners that influence its steady-state redox distribution. It is possible that this undefined reactivity is the reason for the increased trapping of mixed-disulfide partners

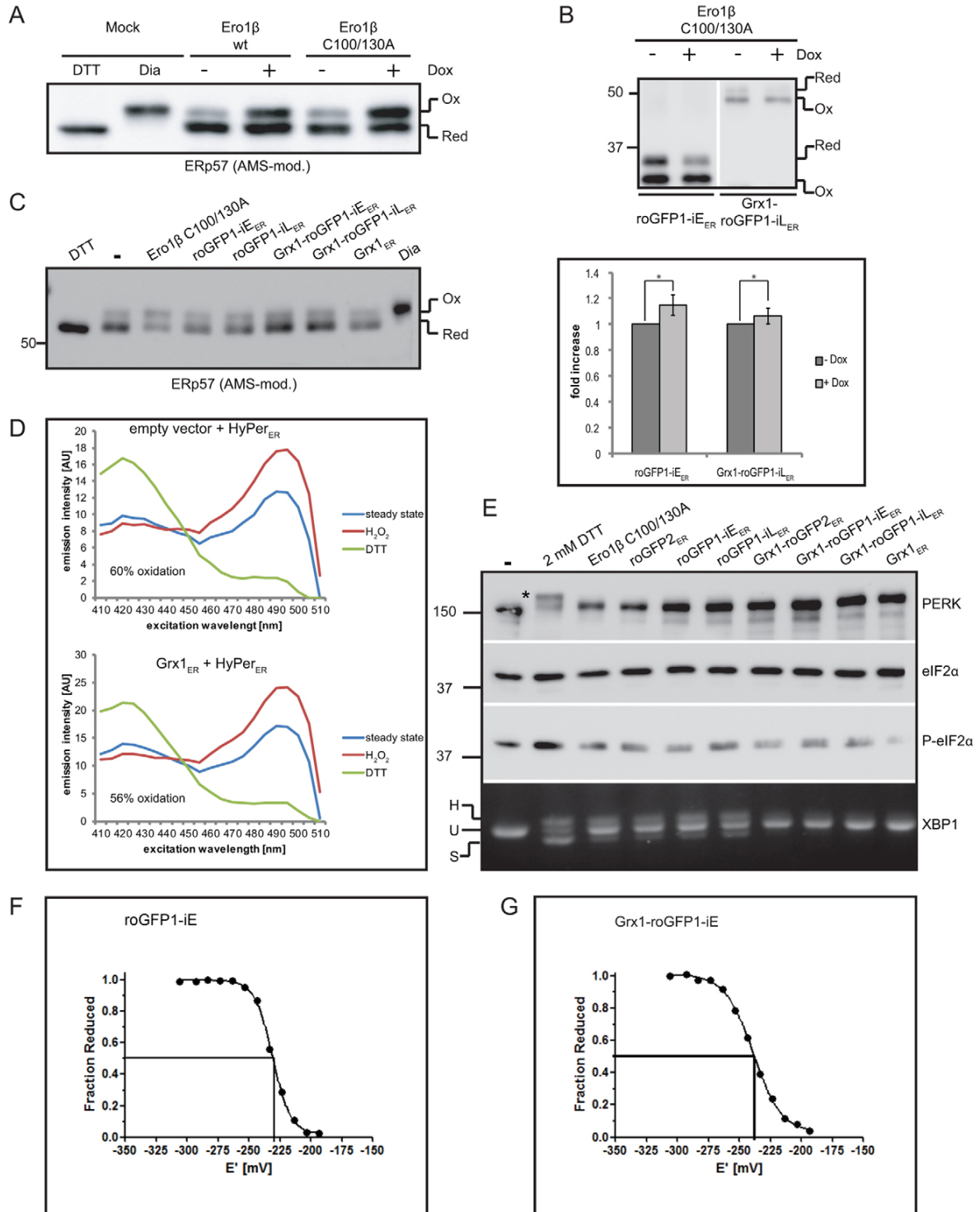


Fig. 6. See next page for legend.

with roGFP1-iX_{ER} compared to Grx1-roGFP1-iX_{ER} (Fig. 4). Likewise, as per Ero1 β -C100/130A, we noticed detectable levels of spliced XBPI mRNA upon expression of unfused roGFPs (Fig. 6E).

Given $E_{\text{GSH}}(\text{ER})$ of -208 ± 4 mV and E'_{GSH} of -240 mV (Rost and Rapoport, 1964), the Nernst equation returns a value for $[\text{GSH}]^2: [\text{GSSG}]$. Accordingly, tentative calculation with a molar GSH:GSSG ratio of 6:1 (Dixon et al., 2008) yields a $[\text{GSx}]_{\text{ER}}$ of 19 ± 6 mM. Notably, this concentration would be significantly higher than the concentration measured in rat liver microsomes [4.5 mM (Dixon et al., 2008)] and in whole HeLa cells [~ 7 mM (van der Schans et al., 1986)]. In the light of the ability of GSH to diffuse through microsomal membranes (Bánhegyi et al., 1999), the former discrepancy may not be surprising. As for a presumably higher $[\text{GSx}]$ in the ER than in the rest of the cell, there are two non-mutually exclusive explanations: (i) Cellular glutathione is trapped in the ER, and/or (ii) the GSH:GSSG ratio in the ER of live cells is greater than 6:1. Specifically measuring this ratio *in situ* is an important future challenge.

PDIs rapidly react with GSH–GSSG *in vitro* (Ruddock, 2012). It was therefore unexpected that the obtained $E_{\text{GSH}}(\text{ER})$ was apparently not oxidizing enough to maintain the known steady-state redox states of PDIs. For instance, the a' domain in ERp57 is typically 15–40% oxidized in cells (Appenzeller-Herzog et al., 2008) (see also Fig. 6C). However, calculation of the oxidized fraction of ERp57a' using its E' [-156 mV (Frickel et al., 2004)] and $E_{\text{GSH}}(\text{ER})$ (i.e. assuming quasi-equilibrium with GSH–GSSG) yields a value of 2%. This indicates that oxidation of ERp57a' is specifically catalyzed and that, at variance with previous models (Appenzeller-Herzog, 2011), GSSG-driven oxidation of reduced PDIs is probably a minor pathway (at least in HeLa cells). Whether the oxidized fraction of ERp57a' [and of other family members such as TMX3 (Haugstetter et al.,

2005)] is maintained by Ero1 (Ramming and Appenzeller-Herzog, 2012) or by other oxidative pathways (Ruddock, 2012) is presently unclear. Another interesting implication following the determination of $E_{\text{GSH}}(\text{ER})$ relates to the question, how a catalytically active (i.e. reduced) fraction of reducing ER oxidoreductases such as Sep15 [$E' = -225$ mV (Ferguson et al., 2006)] can be maintained. Here, equilibration with GSH–GSSG would be expected to result in a reduced fraction of 21%.

Our results also demonstrated differences between roGFP1-iE_{ER} and roGFP1-iL_{ER}, with the latter being less stable, less efficiently folded, less fluorescent and more prone to form mixed-disulfide complexes (Figs 3, 4; supplementary material Fig. S4A). Together with the implementation of codon-optimized cDNAs, this likely means that the expression of roGFP1-iE_{ER} sensors used herein is preferable to that of the previously used roGFP1-iL-KDEL (van Lith et al., 2011). It is conceivable that weak expression of the latter sensor and the concomitant necessity to use strong illumination produced the reported photo-oxidation phenomenon (van Lith et al., 2011), which we never observed in our setup.

ER re-oxidation following the washout of DTT is a rapid process, which takes less than five minutes and depends on Ero1 α (Appenzeller-Herzog et al., 2010; van Lith et al., 2011; Rutkevich and Williams, 2012). Although PDI is the principal substrate of Ero1 α (Inaba et al., 2010; Ramming and Appenzeller-Herzog, 2012), evidence exists that, unlike at steady state (see above), other family members such as ERp57 are also oxidized via Ero1 α during early time points of recovery after DTT (when Ero1 α is maximally active) (Appenzeller-Herzog et al., 2010). In agreement with this, ERp57 reacquires its steady-state redox distribution within seconds in an Ero1 α -dependent manner (Appenzeller-Herzog et al., 2010). By contrast, Grx1-roGFP1-iE_{ER} was re-oxidized within around two minutes (Fig. 7B; supplementary material Fig. S7), which likely reflected its inability to accept disulfide bonds directly from Ero1 α . As expected for a glutathione-specific probe, the kinetics of sensor re-oxidation rather corresponded to the re-oxidation kinetics of GSH–GSSG (Appenzeller-Herzog et al., 2010). In case of roGFP1-iE_{ER} or Grx1SS-roGFP1-iE_{ER}, oxidative recovery was slower compared to Grx1-roGFP1-iE_{ER}. Indeed, as recently modeled (Ruddock, 2012), 'generic' protein disulfides such as these are expected to form at a slower rate upon DTT washout than GSSG.

It has been suggested that UPR signaling following ER stress favors a more reduced ER to promote a more 'cautious' state where release of misfolded proteins is prevented at the expense of an overall diminished secretion rate (Delic et al., 2012). This model was based on yeast strains, which expressed ER-targeted roGFP and were modified to signal an ER stress response (Merksamer et al., 2008; Delic et al., 2012). In keeping with published HyPer_{ER} experiments in HeLa cells (Enyedi et al., 2010), we also observed a swift drop in probe oxidation following inhibition of the ER Ca²⁺ pump (Fig. 8A), which is known to trigger the UPR. While evidence has been presented that ER redox conditions impact on Ca²⁺ handling at the ER membrane (Li and Camacho, 2004; Higo et al., 2005; Anelli et al., 2012), the mechanism underlying this opposite finding is not yet known. Whether or not it depends on the UPR, remains to be determined. However, in agreement with recent findings in pancreatic β -cells (Schuiki et al., 2012), we did not observe ER hypo-oxidation following treatment of cells with another ER stress inducer, TM (Fig. 8B). By contrast, roGFP2 expressed in the ER of yeast cells was massively reduced in response to TM

Fig. 6. Expression of Grx1 in the ER does not measurably change ER redox homeostasis. (A) Mock, Ero1 β wt or Ero1 β -C100/130A cells were, where indicated, induced with 1 $\mu\text{g}/\text{ml}$ doxycycline (Dox) for 24 h or treated with DTT or diamide (Dia). The redox distribution of ERp57 was visualized by WB after differential modification of cellular proteins with NEM and AMS (AMS-mod). Oxidized and reduced forms are indicated. (B) Ero1 β -C100/130A cells were transfected with roGFP1-iE_{ER} or Grx1-roGFP1-iL_{ER} and treated or not with doxycycline (Dox) for 24 h. The cells were then processed as in Fig. 1B. The amount of oxidized versus total protein was quantified by densitometry and the fold increase over uninduced cells plotted (average \pm s.d.; $n=3$) along with 95% confidence intervals as calculated by using a linear model to correct for variation between experimental batches. Asterisks indicate statistical significance ($P<0.04$). (C) HeLa cells were mock-transfected (–) or transfected with the indicated cDNAs. The redox state of ERp57 was determined as in A. (D) HeLa cells were transfected with a mixture of pcDNA3 and HyPer_{ER} or Grx1_{ER} and HyPer_{ER} (plasmid ratio 3:1), and subjected to excitation spectrum analysis. Percentage oxidation at steady state (indicated below the spectra) was calculated from emission intensities at 420 and 500 nm excitation. One of two independent experiments is shown. AU, arbitrary units. (E) HeLa cells transfected with the indicated constructs were subjected to WB against ER stress markers [PERK and phospho (P)-eIF2 α] or to PCR analysis of XBPI splicing. As a positive control for ER stress, HeLa cells were treated with 2 mM DTT for 1 h. Asterisk, phosphorylated form of PERK; U, unspliced form; S, spliced form; H, hybrid form (Shang and Lehman, 2004). (F,G) The standard reduction potentials of purified roGFP1-iE (F) and Grx1-roGFP1-iE (G) were measured as -233 ± 5 mV and -239 ± 3 mV, respectively, as described in the Materials and Methods section. The titration of each protein was carried out three times with four technical replicates.

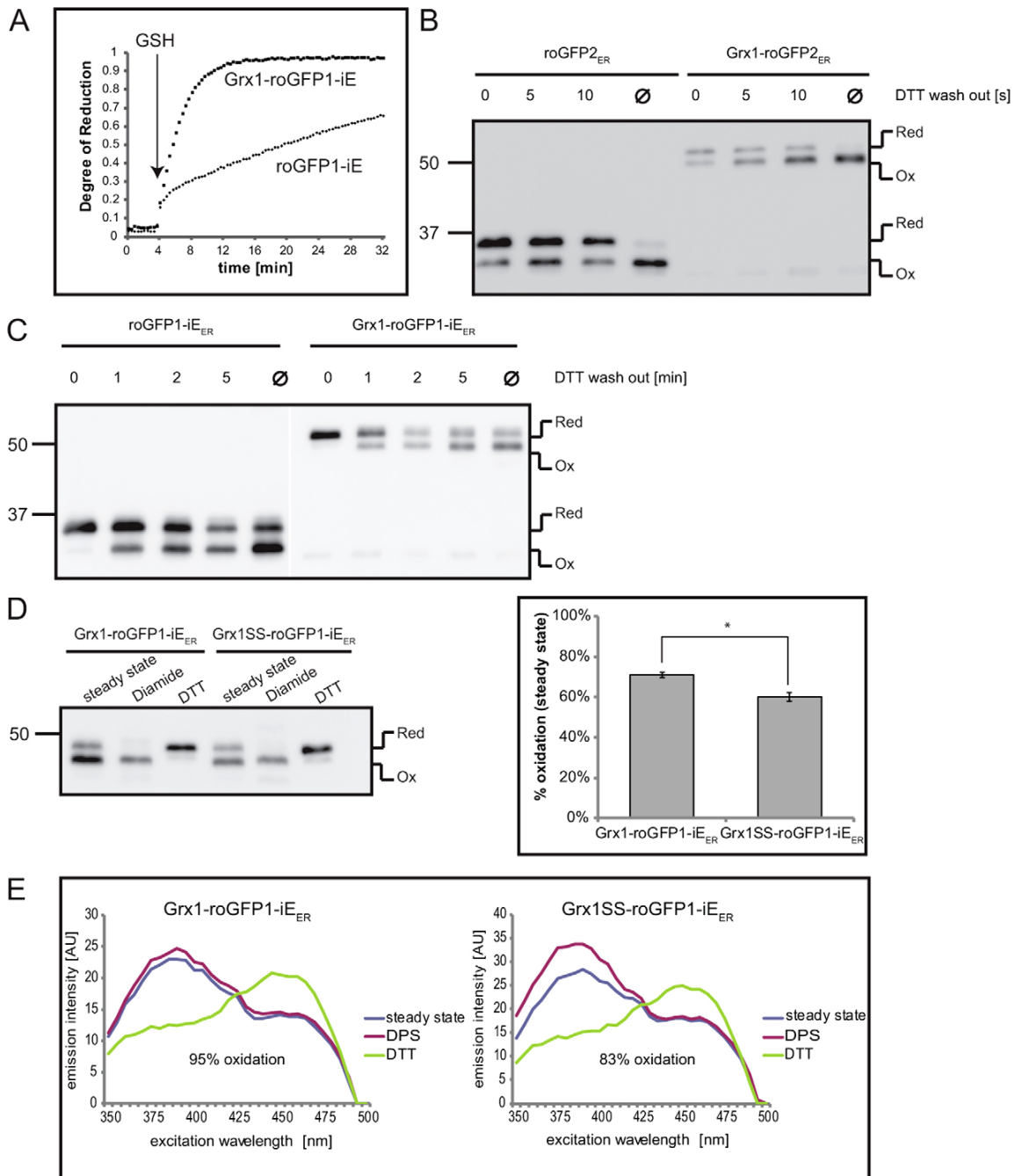


Fig. 7. The catalytic activity of Grx1 enhances equilibration of Grx1-roGFP1-iE_{ER} with GSH-GSSG. (A) Reduction kinetics of purified roGFP1-iE and Grx1-roGFP1-iE was studied in real-time in a fluorescence plate reader upon injection of GSH. (B,C) HeLa cells were transfected with (B) roGFP2_{ER} or Grx1-roGFP2_{ER} or (C) roGFP1-iE_{ER} or Grx1-roGFP1-iE_{ER}, treated with 1 mM DTT and, upon removal of the reductant, incubated in PBS for the times indicated. The Red:Ox ratio of roGFPs was analyzed by IP/WB as in Fig. 1B. (D) Cells transfected with Grx1-roGFP1-iE_{ER} or Grx1SS-roGFP1-iE_{ER} (C23S+C26S) were processed as in Fig. 1B. The degree of sensor oxidation as a percentage was quantified by densitometry (average \pm s.d.; $n=3$). The asterisk indicates statistical significance ($P<0.003$). (E) Cells transfected with Grx1-roGFP1-iE_{ER} or Grx1SS-roGFP1-iE_{ER} were processed as in Fig. 3A. Percentage oxidation at steady state is indicated below the spectra. One of two independent experiments is shown. AU, arbitrary units; Ox, oxidized; Red, reduced.

(Merksamer et al., 2008), which might potentially be explained by ER-stress-induced relocation of this sensor to the cytosol (Rubio et al., 2011).

Several human diseases are caused (or at least accompanied) by manifestations of ER stress and oxidative injury (Kim et al., 2008). In some cases, PDI has been identified as a cytoprotective

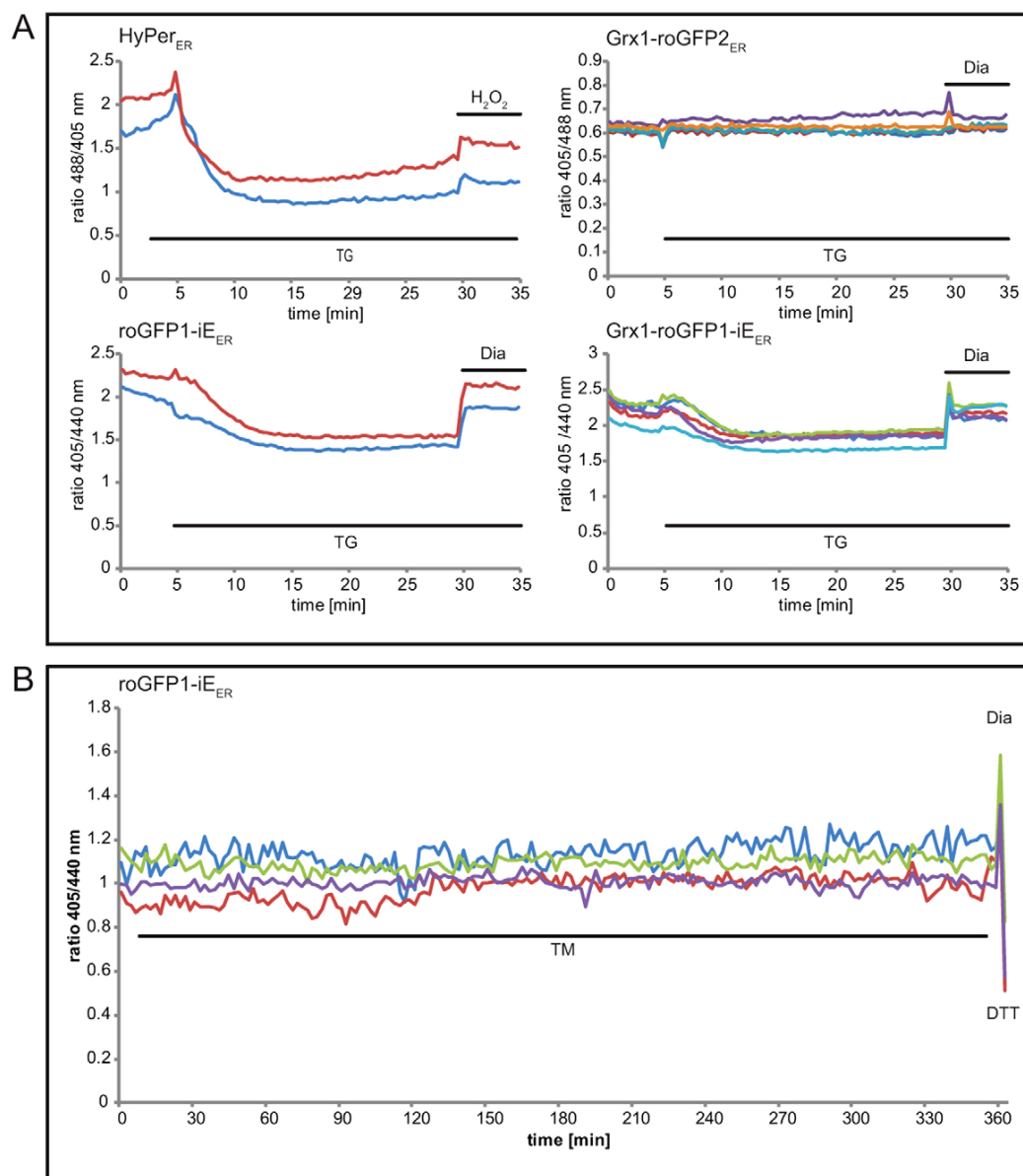


Fig. 8. Real-time monitoring of ER redox changes. HeLa cells were transfected with the indicated constructs and subjected to ratiometric laser scanning microscopy on a temperature-controlled stage with CO₂ control. Fluorescence ratio changes were monitored over time. Each trace corresponds to the data recorded from one cell. (A) The cells were treated with 200 nM thapsigargin (TG) followed by the application of 100 μ M H₂O₂ or 500 μ M diamide (Dia). (B) Where indicated, 1 μ g/ml tunicamycin (TM), 0.5 mM diamide (Dia) and 20 mM DTT were added to the specimen. One of at least two independent experiments is shown.

factor, indicating that modulation of the ER thiol–disulfide system including E_{GSH}(ER) confers therapeutic advantage (Tanaka et al., 2000; Severino et al., 2007; Walker et al., 2010; Wang et al., 2012). By developing a glutathione-responsive ER sensor, which allows an authentic estimate of E_{GSH}(ER) in living cells, this study now offers an important tool to study these processes *in vivo*. It will be interesting to test, whether there is a direct relationship between changes in E_{GSH}(ER) and the survival rate of cells experiencing pathological ER stress.

Materials and Methods

Recombinant DNA

Cloning of Grx1-roGFP2_{ER} was initiated by amplifying the coding sequence from pLPCX/Grx1-roGFP2 (Gutscher et al., 2008) and extending it to encode KDEL* at the C-terminus using 5'-GAA GGT ACC ATG GCT CAA GAG TTT GTG AAC TGC-3' and 5'-GGT GAA GCT TTT ACA GTT CGT CCT TGT ACA GCT CGT CCA TGC-3' (Restriction sites underlined). The PCR product was ligated via Asp718/*Hind*III into a plasmid harboring the ER signal sequence of ERp44 and an HA epitope upstream of an Asp718 site (Otsu et al., 2006). To obtain Grx1-roGFP1-iX_{ER} constructs, Grx1-roGFP2_{ER} was mutated by the QuikChange protocol (Stratagene) as follows (only sense strand primers, mutations

underlined, amino acid numbers derived from roGFP): iE insertion [C147CE+H148S; (Lohman and Remington, 2008)]: 5'-GGA GTA CAA CTA CAA CTG CGA GAG CAA CGT CTA TAT CAT GG-3'; iL insertion (C147CL+H148S): 5'-GGA GTA CAA CTA CAA CTG CCT GAG CAA CGT CTA TAT CAT GG-3'; T65S: 5'-CGT GAC CAC CCT GAG CTA CGG CGT GC-3'; F99S: 5'-GGA GCG CAC CAT CAG CTT CAA GGA CGA CGG C-3'; M153T: 5'-GCA ACG TCT ATA TCA CCG CCG ACA AGC AGA AGA ACG-3'; V163A+H167T: 5'-GAA GAA CGG CAT CAA GGC TAA CTT CAA GAC CCG C-3'. To obtain roGFP1-iX_{ER}, the roGFP moiety was amplified from Grx1-roGFP1-iX_{ER} using 5'-AGA GGT ACC GTG AGC AAG GGC GAG GAG-3' and 5'-GGT GAA GCT TTT ACA GTT CGT CCT TGT ACA GCT CGT CCA TGC-3' and cloned via Asp718/*Hind*III as described above.

WtGFP(jellyfish)-derived roGFP1-iE_{ER} constructs were generated by amplifying the coding sequence from pQ30/roGFP1-iE [obtained by QuikChange (5'-TTG GAA TAC AAC TAT AAC TGC GAG TCC AAT GTA TAC ATC ACG GCA-3')] using pQ30/roGFP1-iL (Lohman and Remington, 2008) as template] using 5'-GAA GGT ACC AGT AAG GGA GAA GAA CTT TTC ACT GG-3' and 5'-AGA CTT AAG TTA CAG TTC GTC TTT GTA TAG TTC ATC CAT GCC ATG T-3'. The resulting fragment (featuring a KDEL* motif) was then ligated into Asp718/*Afl*III-digested pcDNA3.1-ERp57-HA (see above). N-terminal fusion with Grx1 was achieved by excising roGFP1-iE_{ER} with *Eco*R1/*Afl*III and exchanging it with the roGFP1-iL sequence in Grx1-roGFP1-iL_{ER}. For the cloning of pQE-30/Grx1-roGFP1-iE, *Bam*HI sites at the 5' end of Grx1 and the 3' end of the glycine-serine linker were introduced into Grx1-roGFP1-iE_{ER} by QuikChange (sense strand primers 5'-CCT GAC TAC GCA GAA GGA TCC ATG GCT CAA GAG TTT G-3' and 5'-GAT CAG GAG GAG GAT CCG TGA GCA AGG GCG-3'), and the resulting cDNA digested with *Bam*HI to generate Grx1-GSGG₆, which was ligated into *Bam*HI-digested pQE-30/roGFP1-iE.

Grx1_{ER} was amplified from Grx1-roGFP2_{ER} using 5'-GAA GGT ACC ATG GCT CAA GAG TTT GTG AAC TGC-3' and 5'-GCA AGC TTT TAC AGT TCG TCC TTC TGC AGA GCT CCA ATC TGC TTT A-3' and ligated into Asp718/*Hind*III-digested pcDNA3.1-ERp57-HA (see above). The N52Q and C23S+C26S mutants of Grx1-roGFP1-iE_{ER} were generated by QuikChange (sense strand primers: 5'-CGA TAT CAC AGC CAC CCA GCA CAC TAA CGA GAT TCA AG-3' and 5'-CAT CAA GCC CAC CTC TCC GTA CTC CAG GAG GGC CCA AG-3'). PcDNA5/FRT/TO/Ero1β-C100/T30A was obtained by introducing C100A and C130A (sense strand primers: 5'-GAC TGT CAT GTG GAG CCC GCA CCA GAG AGT AAA ATT CCG-3' and 5'-GGC AAA CAA TAC CAA AGA ATT AGA AGA TGC TGA GCA AGC TAA TAA ACT GGG-3') into pcDNA5/Ero1βmyc6his (Appenzeller-Herzog et al., 2008) by QuikChange.

Cell culture and transient transfection

HeLa cells were cultivated in Dulbecco's Modified Eagle's Medium (DMEM) containing 4.5 g/l glucose supplemented with 10% fetal bovine serum, 100 U/ml penicillin, 100 μg/ml streptomycin at 37°C in 5% CO₂. HeLa cells were transfected with Turbofect (Fermentas) or, for microscopy and fluorescence scanning, with Fugene HD (Promega) according to the manufacturers' protocols. Flp-in TRex 293 cells stably transfected with empty vector (Mock) or wild-type Ero1β have been described previously (Appenzeller-Herzog et al., 2008). A corresponding cell line inducibly expressing Ero1β-C100/T30A was generated as suggested by Invitrogen. Flp-in TRex 293-derived cell lines were transfected with Metafectene PRO (Biontex).

Pulse-chase analysis

Transfected cells were starved for 15 min in DMEM without methionine and cysteine (Sigma). Subsequently the cells were labeled with 100 μCi/ml [³⁵S]protein labeling mix (PerkinElmer) and chased in normal growth medium containing 10 mM L-methionine for indicated times. Cells were washed once with PBS containing 20 mM N-ethylmaleimide (NEM), incubated in the same buffer for 20 min on ice, and then subjected to denaturing anti-HA immunoprecipitation as described elsewhere (Appenzeller-Herzog et al., 2005). Bound proteins were analyzed by non-reducing SDS-PAGE and autoradiography.

Immunoprecipitation, western blot, washout experiments and AMS modification

To obtain completely reduced or oxidized control samples, cells were pretreated with either 10 mM DTT or 5 mM diamide in normal growth medium for 5 min at 37°C. Cells were then washed with phosphate buffered saline (PBS) containing 20 mM NEM and incubated in the same buffer for 20 min on ice. The cells were lysed on ice for 1 h in 100 mM NaPO₄, pH 8, containing 1% Triton-X-100 and 200 μM phenylmethylsulfonyl fluoride. Insoluble cell debris were pelleted for 1 h at 4°C and 16,000 g, and the supernatant was immunoprecipitated using NHS-activated agarose (Thermo Scientific) decorated with anti-GFP (Kojer et al., 2012) (generously provided by Jan Riemer, University of Kaiserslautern, Germany). Primary antibodies used for WB were anti-HA (a kind gift from Hans-Peter Hauri University of Basel, Switzerland), anti-ERp57 (a kind gift from Ari Helenius, ETH Zürich, Switzerland), anti-PERK, anti-eIF2α and anti-P-eIF2α (Cell Signaling Technology). DTT and diamide washout experiments were performed as described

previously (Appenzeller-Herzog et al., 2010). Where indicated, diamide was replaced by 1 mM DPS. AMS modification of originally disulfide-bound cysteines is delineated elsewhere (Appenzeller-Herzog and Ellgaard, 2008).

Fluorescence spectrum analysis

For roGFP measurements, HeLa cells were trypsinized 48 h post transfection and washed twice in HEPES buffer (20 mM HEPES pH 7.4, 130 mM NaCl, 5 mM KCl, 1 mM CaCl₂, 1 mM MgCl₂, 5.5 mM D-glucose). A total of 3×10⁵ cells per well were seeded in HEPES buffer onto a flat-bottom 96-well plate. Plates were briefly centrifuged at 180×g and the cells were left untreated or treated with 0.5 mM DPS or 10 mM DTT (three wells per condition). Fluorescence intensities at 530 nm emission were measured from the bottom on a Spectramax Gemini EM (Molecular Device) within a 350–500 nm excitation range. HyPer_{ER} (Enyedi et al., 2010) (kindly provided by Miklos Geiszt, Semmelweis University, Hungary) measurements were performed within a 410–510 nm excitation range at 535 nm emission, using 100 μM H₂O₂ instead of DPS, and omitting D-glucose from the buffer.

Live-cell microscopy and image analysis

Cells were grown on glass bottom dishes (Ibidi). For determination of the extent of sensor oxidation, roGFP-expressing cells were washed twice with HEPES buffer and the dishes transferred to an Olympus Fluoview 1000 laser scanning confocal microscope equipped with a 60×oil immersion objective (NA 1.40) and a 405 nm laser diode, a 440 nm laser diode, and a 488 nm argon laser. Pictures (1024×1024 pixels) were taken with an open pinhole within an emission window of 505–605 nm at steady state, 1 min after addition of 5 mM diamide, and 5 min after addition of 20 mM DTT. One region of interest (ROI) per cell was chosen, which remained immobile for the duration of image acquisition, and 405/440 or 405/488 nm ratios were determined from average intensities in background-subtracted ROIs. False color images were generated using the Fluoview 1000 software. For time-lapse imaging, cells were washed twice with DMEM without phenol red and subjected to ratiometric laser scanning microscopy using a stage incubator (37°C), CO₂ control, a 20/80 excitation and a 50/50 emission beam splitter. Fluorographs were analyzed with the ImageJ software.

XBp1 splicing assay

Total RNA was extracted from HeLa cells using TRI Reagent (Sigma), and reverse transcribed with Superscript III (Invitrogen). The resulting cDNA was subjected to PCR using 5'-AAA CAG AGT AGC TCA GAC TGC-3' and 5'-TCC TTC TGG GTA GAC CTC TGG GAG-3' to generate XBp1 amplicons, which were separated on a 2% agarose gel.

Calculation of reduction potentials

Based on *in situ* fluorescence data, the degree of sensor oxidation (OxD) for the different roGFP_{ER} sensors was determined using the following equation (using 488 nm or 440 nm for the excitation of the red-shifted 'B-form' of roGFP2_{ER} or roGFP1-iX_{ER}, respectively):

$$OxD_{roGFP} = \frac{R - R_{red}}{\frac{I(B)_{min}}{I(B)_{max}}(R_{ox} - R) + (R - R_{red})}$$

where R, R_{red} and R_{ox} represent the 405:488/440 nm fluorescence ratios at steady state, upon complete reduction or oxidation, respectively, and I(B)_{min} and I(B)_{max} the fluorescence intensities of fully oxidized and fully reduced roGFP measured with excitation of the B form at either 488 or 440 nm. In the case of live-cell imaging, the calculation of OxD was done separately for every cell, and the values were averaged. To express the full oxidation of roGFP_{ER} measured in a subset of cells, OxD was arbitrarily set to 1.

Using OxD, the reduction potential of Grx1-roGFP1-iE_{ER} was calculated using the Nernst equation:

$$E_{roGFP} = E^0_{roGFP} - \frac{RT}{2F} \ln \left(\frac{1 - OxD_{roGFP}}{OxD_{roGFP}} \right)$$

with E⁰ = -239 mV (Fig. 6G). R is the gas constant (8.315 J K⁻¹ mol⁻¹), T the temperature (298 K), and F the Faraday constant (96485 C mol⁻¹). Assuming complete equilibrium between Grx1-roGFP1-iE_{ER} and GSH-GSSG, E_{GSH(ER)} equals E_{Grx1-roGFP1-iE-ER}.

Indirect immunofluorescence staining

Transiently transfected HeLa cells were grown for 48 h on glass coverslips, fixed with 4% paraformaldehyde for 20 min at room temperature, quenched with 50 mM NH₄Cl and permeabilized with 0.1% Triton X-100. The cells were blocked with 1% BSA in PBS and incubated in the same buffer with anti-PDI (RL90, Abcam; 1:100) or anti-HA (1:1000) for 1 h at room temperature. The coverslips were washed with PBS and incubated with a goat-anti-mouse Hilyte 555

conjugated antibody (AnaSpec). After several washes with PBS, the cells were mounted in Mowiol 4-88 (Hoechst). Staining was analyzed on an Olympus Fluoview 1000 laser scanning confocal microscope (pinhole: 80 μm).

Experiments with purified proteins

N-terminally hexahistidine-tagged Grx1-roGFP1-iE and roGFP1-iE were purified as reported elsewhere (Meyer et al., 2007). To get their standard (midpoint) potentials, the sensors (1 μM final concentration) were equilibrated for 2–3 h with defined mixtures of oxidized/reduced lipoic acid (2.5 mM) in degassed 100 mM HEPES pH 7.0, 300 mM NaCl, 1 mM EDTA. From the fluorescence intensities at 520 nm for excitation at 390 and 480 nm, respectively, as determined on a fluorescence plate reader (POLARstar Omega; BMG, <http://www.bmg-labtech.com>) with filter-based excitation, $\text{OxDr}_{\text{roGFP}}$ values were derived as described above. 1-OxD (RedD) was plotted against the potentials of the respective lipoic acid redox buffers. Single data points were fitted to a sigmoidal dose-response curve using GraphPadPrism5 (GraphPad Software, San Diego California USA) to calculate E' of both sensors using $E'_{\text{lipoic acid of } -290 \text{ mV}}$ (Lees and Whitesides, 1993).

Ratiometric time-course measurements with isolated protein were performed as described previously (Meyer et al., 2007). Briefly, glutathione solutions were automatically injected to a final concentration of 2 mM into phosphate-buffered solutions of roGFP (1 μM), 0.1 μM recombinant Glutathione Reductase (Sigma) and 100 μM NADPH. The sensors were pre-oxidized for 30 min with 10 mM H_2O_2 , which was then removed by ZebaTM Spin Desalting Columns. H_2O_2 and DTT to a final concentration of 10 mM were separately used to define maximum oxidation and maximum reduction of the sensors.

Statistical analysis

Data sets were analyzed for statistical significance using Student's *t*-test. To evaluate the relative changes in the roGFP redox ratios upon induction of Ero1 β -C100/130A, the data from different experimental batches were logarithmically transformed and fitted to a linear model using a batch specific offset value. Linear regression, 95% confidence intervals, and P values were calculated using Microsoft Excel.

Acknowledgements

We thank Lars Ellgaard for help with Ero1 experiments, Anne Spang for critical reading of the manuscript, and Jim Remington, Miklos Geiszt, Jan Riemer, Ari Helenius, and Hans-Peter Hauri for reagents.

Author contributions

J.B. performed and analyzed most of the experiments. M.M. performed molecular cloning, fluorescence scanning, and WB experiments. I.A. conducted experiments with purified proteins with input from A.J.M.. H.G.H. generated the Ero1 β -C100/130A cell line and contributed Fig. 6A. A.O. contributed reagents/materials/analytical tools. C.A.-H. performed experiments, conceived, and supervised the study. J.B. and C.A.-H. analyzed the data and wrote the manuscript with input from T.P.D. and A.J.M.

Funding

This work was funded by the Ambizione program of the Swiss National Science Foundation (PZ00P3_126625/1 to C.A.-H.); the Swiss Center for Applied Human Toxicology (to A.O.); the University of Basel (to C.A.-H. and A.O.); and the August Collin-Fonds (to C.A.-H.).

Supplementary material available online at

<http://jcs.biologists.org/lookup/suppl/doi:10.1242/jcs.117218/-/DC1>

References

Anelli, T., Bergamelli, L., Margittai, E., Rimessi, A., Fagioli, C., Malgaroli, A., Pinton, P., Ripamonti, M., Rizzuto, R. and Sitia, R. (2012). Ero1 α regulates Ca^{2+} fluxes at the endoplasmic reticulum-mitochondria interface (MAM). *Antioxid. Redox Signal.* **16**, 1077–1087.

Appenzeller-Herzog, C. (2011). Glutathione- and non-glutathione-based oxidant control in the endoplasmic reticulum. *J. Cell Sci.* **124**, 847–855.

Appenzeller-Herzog, C. (2012). Updates on “endoplasmic reticulum redox”. *Antioxid. Redox Signal.* **16**, 760–762.

Appenzeller-Herzog, C. and Ellgaard, L. (2008). In vivo reduction-oxidation state of protein disulfide isomerase: the two active sites independently occur in the reduced and oxidized forms. *Antioxid. Redox Signal.* **10**, 55–64.

Appenzeller-Herzog, C., Nyfeler, B., Burkhard, P., Santamaria, I., Lopez-Otin, C. and Hauri, H. P. (2005). Carbohydrate- and conformation-dependent cargo capture for ER-exit. *Mol. Biol. Cell* **16**, 1258–1267.

Appenzeller-Herzog, C., Riemer, J., Christensen, B., Sørensen, E. S. and Ellgaard, L. (2008). A novel disulphide switch mechanism in Ero1 α balances ER oxidation in human cells. *EMBO J.* **27**, 2977–2987.

Appenzeller-Herzog, C., Riemer, J., Zito, E., Chin, K.-T., Ron, D., Spiess, M. and Ellgaard, L. (2010). Disulphide production by Ero1 α -PDI relay is rapid and effectively regulated. *EMBO J.* **29**, 3318–3329.

Bánhegyi, G., Lusini, L., Puskás, F., Rossi, R., Fulceri, R., Braun, L., Mile, V., di Simplicio, P., Mandl, J. and Benedetti, A. (1999). Preferential transport of glutathione versus glutathione disulfide in rat liver microsomal vesicles. *J. Biol. Chem.* **274**, 12213–12216.

Bass, R., Ruddock, L. W., Klappa, P. and Freedman, R. B. (2004). A major fraction of endoplasmic reticulum-located glutathione is present as mixed disulfides with protein. *J. Biol. Chem.* **279**, 5257–5262.

Belousov, V. V., Fradkov, A. F., Lukyanov, K. A., Staroverov, D. B., Shakhbazov, K. S., Terskikh, A. V. and Lukyanov, S. (2006). Genetically encoded fluorescent indicator for intracellular hydrogen peroxide. *Nat. Methods* **3**, 281–286.

Braakman, I. and Bulleid, N. J. (2011). Protein folding and modification in the mammalian endoplasmic reticulum. *Annu. Rev. Biochem.* **80**, 71–99.

Brejci, K., Sixma, T. K., Kitts, P. A., Kain, S. R., Tsien, R. Y., Ormó, M. and Remington, S. J. (1997). Structural basis for dual excitation and photoisomerization of the Aequorea victoria green fluorescent protein. *Proc. Natl. Acad. Sci. USA* **94**, 2306–2311.

Chakravarthi, S., Jessop, C. E. and Bulleid, N. J. (2006). The role of glutathione in disulphide bond formation and endoplasmic-reticulum-generated oxidative stress. *EMBO Rep.* **7**, 271–275.

Delic, M., Rebnecker, C., Wanka, F., Puxbaum, V., Haberhauer-Troyer, C., Hann, S., Köllensperger, G., Mattanovich, D. and Gasser, B. (2012). Oxidative protein folding and unfolded protein response elicit differing redox regulation in endoplasmic reticulum and cytosol of yeast. *Free Radic. Biol. Med.* **52**, 2000–2012.

Dixon, B. M., Heath, S. H., Kim, R., Suh, J. H. and Hagen, T. M. (2008). Assessment of endoplasmic reticulum glutathione redox status is confounded by extensive ex vivo oxidation. *Antioxid. Redox Signal.* **10**, 963–972.

Dooley, C. T., Dore, T. M., Hanson, G. T., Jackson, W. C., Remington, S. J. and Tsien, R. Y. (2004). Imaging dynamic redox changes in mammalian cells with green fluorescent protein indicators. *J. Biol. Chem.* **279**, 22284–22293.

Enyedi, B., Várnai, P. and Geiszt, M. (2010). Redox state of the endoplasmic reticulum is controlled by Ero1L- α and intraluminal calcium. *Antioxid. Redox Signal.* **13**, 721–729.

Ferguson, A. D., Labunskyy, V. M., Fomenko, D. E., Araç, D., Chelliah, Y., Amezcua, C. A., Rizo, J., Gladyshev, V. N. and Deisenhofer, J. (2006). NMR structures of the selenoproteins Sep15 and SelM reveal redox activity of a new thioredoxin-like family. *J. Biol. Chem.* **281**, 3536–3543.

Frickel, E. M., Frei, P., Bouvier, M., Stafford, W. F., Helenius, A., Glockshuber, R. and Ellgaard, L. (2004). ERp57 is a multifunctional thiol-disulfide oxidoreductase. *J. Biol. Chem.* **279**, 18277–18287.

Gutschner, M., Pauleau, A.-L., Marty, L., Brach, T., Wabnitz, G. H., Samstag, Y., Meyer, A. J. and Dick, T. P. (2008). Real-time imaging of the intracellular glutathione redox potential. *Nat. Methods* **5**, 553–559.

Haas, J., Park, E. C. and Seed, B. (1996). Codon usage limitation in the expression of HIV-1 envelope glycoprotein. *Curr. Biol.* **6**, 315–324.

Hansen, R. E. and Winther, J. R. (2009). An introduction to methods for analyzing thiols and disulfides: Reactions, reagents, and practical considerations. *Anal. Biochem.* **394**, 147–158.

Hansen, R. E., Roth, D. and Winther, J. R. (2009). Quantifying the global cellular thiol-disulfide status. *Proc. Natl. Acad. Sci. USA* **106**, 422–427.

Hansen, H. G., Schmidt, J. D., Soltfoft, C. L., Ramming, T., Geertz-Hansen, H. M., Christensen, B., Sørensen, E. S., Juncker, A. S., Appenzeller-Herzog, C. and Ellgaard, L. (2012). Hyperactivity of the Ero1 α oxidase elicits endoplasmic reticulum stress but no broad antioxidant response. *J. Biol. Chem.* **287**, 39513–39523.

Hanson, G. T., Aggeler, R., Oglesbee, D., Cannon, M., Capaldi, R. A., Tsien, R. Y. and Remington, S. J. (2004). Investigating mitochondrial redox potential with redox-sensitive green fluorescent protein indicators. *J. Biol. Chem.* **279**, 13044–13053.

Haugstetter, J., Blicher, T. and Ellgaard, L. (2005). Identification and characterization of a novel thioredoxin-related transmembrane protein of the endoplasmic reticulum. *J. Biol. Chem.* **280**, 8371–8380.

Hetz, C. (2012). The unfolded protein response: controlling cell fate decisions under ER stress and beyond. *Nat. Rev. Mol. Cell Biol.* **13**, 89–102.

Higo, T., Hattori, M., Nakamura, T., Natsume, T., Michikawa, T. and Mikoshiba, K. (2005). Subtype-specific and ER luminal environment-dependent regulation of inositol 1,4,5-trisphosphate receptor type 1 by ERp44. *Cell* **120**, 85–98.

Hwang, C., Sinskey, A. J. and Lodish, H. F. (1992). Oxidized redox state of glutathione in the endoplasmic reticulum. *Science* **257**, 1496–1502.

Inaba, K., Masui, S., Iida, H., Vavassori, S., Sitia, R. and Suzuki, M. (2010). Crystal structures of human Ero1 α reveal the mechanisms of regulated and targeted oxidation of PDI. *EMBO J.* **29**, 3330–3343.

Izquierdo, A., Casas, C., Mühlenhoff, U., Lillig, C. H. and Herrero, E. (2008). Saccharomyces cerevisiae Grx6 and Grx7 are monothiol glutaredoxins associated with the early secretory pathway. *Eukaryot. Cell* **7**, 1415–1426.

Kim, I., Xu, W. and Reed, J. C. (2008). Cell death and endoplasmic reticulum stress: disease relevance and therapeutic opportunities. *Nat. Rev. Drug Discov.* **7**, 1013–1030.

- Kojar, K., Bien, M., Gangel, H., Morgan, B., Dick, T. P. and Riemer, J. (2012). Glutathione redox potential in the mitochondrial intermembrane space is linked to the cytosol and impacts the Mia40 redox state. *EMBO J.* **31**, 3169-3182.
- Kolossov, V. L., Leslie, M. T., Chatterjee, A., Sheehan, B. M., Kenis, P. J. and Gaskins, H. R. (2012). Förster resonance energy transfer-based sensor targeting endoplasmic reticulum reveals highly oxidative environment. *Exp. Biol. Med. (Maywood)* **237**, 652-662.
- Lees, W. J. and Whitesides, G. M. (1993). Equilibrium-constants for thiol disulfide interchange reactions - a coherent, corrected set. *J. Org. Chem.* **58**, 642-647.
- Li, Y. and Camacho, P. (2004). Ca²⁺-dependent redox modulation of SERCA 2b by ERp57. *J. Cell Biol.* **164**, 35-46.
- Lohman, J. R. and Remington, S. J. (2008). Development of a family of redox-sensitive green fluorescent protein indicators for use in relatively oxidizing subcellular environments. *Biochemistry* **47**, 8678-8688.
- Merksamer, P. I., Trusina, A. and Papa, F. R. (2008). Real-time redox measurements during endoplasmic reticulum stress reveal interlinked protein folding functions. *Cell* **135**, 933-947.
- Meyer, A. J. and Dick, T. P. (2010). Fluorescent protein-based redox probes. *Antioxid. Redox Signal.* **13**, 621-650.
- Meyer, A. J., Brach, T., Marty, L., Kreye, S., Rouhier, N., Jacquot, J.-P. and Hell, R. (2007). Redox-sensitive GFP in *Arabidopsis thaliana* is a quantitative biosensor for the redox potential of the cellular glutathione redox buffer. *Plant J.* **52**, 973-986.
- Østergaard, H., Tachibana, C. and Winther, J. R. (2004). Monitoring disulfide bond formation in the eukaryotic cytosol. *J. Cell Biol.* **166**, 337-345.
- Otsu, M., Bertoli, G., Fagioli, C., Guerini-Rocco, E., Nerini-Molteni, S., Ruffato, E. and Sitia, R. (2006). Dynamic retention of Ero1alpha and Ero1beta in the endoplasmic reticulum by interactions with PDI and ERp44. *Antioxid. Redox Signal.* **8**, 274-282.
- Ramming, T. and Appenzeller-Herzog, C. (2012). The physiological functions of mammalian endoplasmic oxidoreductin 1: on disulfides and more. *Antioxid. Redox Signal.* **16**, 1109-1118.
- Rost, J. and Rapoport, S. (1964). Reduction-Potential of Glutathione. *Nature* **201**, 185.
- Rubio, C., Pincus, D., Korennykh, A., Schuck, S., El-Samad, H. and Walter, P. (2011). Homeostatic adaptation to endoplasmic reticulum stress depends on Ire1 kinase activity. *J. Cell Biol.* **193**, 171-184.
- Ruddock, L. W. (2012). Low-molecular-weight oxidants involved in disulfide bond formation. *Antioxid. Redox Signal.* **16**, 1129-1138.
- Rutkevich, L. A. and Williams, D. B. (2012). Vitamin K epoxide reductase contributes to protein disulfide formation and redox homeostasis within the endoplasmic reticulum. *Mol. Biol. Cell* **23**, 2017-2027.
- Rutkowski, D. T. and Hegde, R. S. (2010). Regulation of basal cellular physiology by the homeostatic unfolded protein response. *J. Cell Biol.* **189**, 783-794.
- Schafer, F. Q. and Buettner, G. R. (2001). Redox environment of the cell as viewed through the redox state of the glutathione disulfide/glutathione couple. *Free Radic. Biol. Med.* **30**, 1191-1212.
- Schuike, I., Zhang, L. and Volchuk, A. (2012). Endoplasmic reticulum redox state is not perturbed by pharmacological or pathological endoplasmic reticulum stress in live pancreatic β -cells. *PLoS ONE* **7**, e48626.
- Severino, A., Campioni, M., Straino, S., Salloum, F. N., Schmidt, N., Herbrand, U., Frede, S., Toietta, G., Di Rocco, G., Bussani, R. et al. (2007). Identification of protein disulfide isomerase as a cardiomyocyte survival factor in ischemic cardiomyopathy. *J. Am. Coll. Cardiol.* **50**, 1029-1037.
- Shang, J. and Lehrman, M. A. (2004). Discordance of UPR signaling by ATF6 and Ire1p-XBP1 with levels of target transcripts. *Biochem. Biophys. Res. Commun.* **317**, 390-396.
- Shimomura, O., Johnson, F. H. and Saiga, Y. (1962). Extraction, purification and properties of aequorin, a bioluminescent protein from the luminous hydromedusa, *Aequorea*. *J. Cell. Comp. Physiol.* **59**, 223-239.
- Sun, C., Berardi, M. J. and Bushweller, J. H. (1998). The NMR solution structure of human glutaredoxin in the fully reduced form. *J. Mol. Biol.* **280**, 687-701.
- Tanaka, S., Uehara, T. and Nomura, Y. (2000). Up-regulation of protein-disulfide isomerase in response to hypoxia/brain ischemia and its protective effect against apoptotic cell death. *J. Biol. Chem.* **275**, 10388-10393.
- van der Schans, G. P., Vos, O., Roos-Verheij, W. S. and Lohman, P. H. (1986). The influence of oxygen on the induction of radiation damage in DNA in mammalian cells after sensitization by intracellular glutathione depletion. *Int. J. Radiat. Biol. Relat. Stud. Phys. Chem. Med.* **50**, 453-465.
- van Lith, M., Tiwari, S., Pediani, J., Milligan, G. and Bulleid, N. J. (2011). Real-time monitoring of redox changes in the mammalian endoplasmic reticulum. *J. Cell Sci.* **124**, 2349-2356.
- Walker, A. K., Farg, M. A., Bye, C. R., McLean, C. A., Horne, M. K. and Atkin, J. D. (2010). Protein disulfide isomerase protects against protein aggregation and is S-nitrosylated in amyotrophic lateral sclerosis. *Brain* **133**, 105-116.
- Wang, L., Zhu, L. and Wang, C. C. (2011). The endoplasmic reticulum sulfhydryl oxidase Ero1 β drives efficient oxidative protein folding with loose regulation. *Biochem. J.* **434**, 113-121.
- Wang, S. B., Shi, Q., Xu, Y., Xie, W. L., Zhang, J., Tian, C., Guo, Y., Wang, K., Zhang, B. Y., Chen, C. et al. (2012). Protein disulfide isomerase regulates endoplasmic reticulum stress and the apoptotic process during prion infection and PrP mutant-induced cytotoxicity. *PLoS ONE* **7**, e38221.
- Yang, T. T., Cheng, L. and Kain, S. R. (1996). Optimized codon usage and chromophore mutations provide enhanced sensitivity with the green fluorescent protein. *Nucleic Acids Res.* **24**, 4592-4593.
- Zito, E., Melo, E. P., Yang, Y., Wahlander, A., Neubert, T. A. and Ron, D. (2010). Oxidative protein folding by an endoplasmic reticulum-localized peroxiredoxin. *Mol. Cell* **40**, 787-797.